Ceram. Int.
2019/1/7 (Revision)

Well-facetted spinel-type Co_3O_4 microcrystal assembly prepared by hydrothermal synthesis and post-thermal decomposition

Kazuki Fukui[a], Yoshikazu Suzuki[a,b]**

[a] Graduate School of Pure and Applied Sciences, University of Tsukuba, Ibaraki 305-8573, Japan

[b] Faculty of Pure and Applied Sciences, University of Tsukuba, Ibaraki 305-8573, Japan

Abstract

Co_3O_4-based materials attract a lot of attention particularly for electrochemical applications. Here, we report a unique Co_3O_4 hierarchical micro- and nanostructures (HMNS), *viz.*, micrometer-sized mesoporous granules assembled with Co_3O_4 facetted nanocrystals. $CoCl_2 \cdot 6H_2O$ and urea (Co : urea = 2:15 in mol fraction) were dissolved in a water/ethanol mixed solution and hydrothermally heated at 160°C for 0.5 h, 4 h and 6 h. The three precursors were calcined at 350°C for 3 h in air atmosphere. The product via hydrothermal treatment for 4 h was composed of 'soft' cube-like granules, which actually was the assembly of well-facetted Co_3O_4 microcrystals with pore-size distribution of ~10-100 nm. The other product via hydrothermal treatment for 6 h was composed of 'hard' cube-like granules, which actually was the assembly of fine and equiaxed Co_3O_4 nanocrystals with narrow pore-size of distribution of ~10 nm. Macro- and mesoporous Co_3O_4 powders with controlled pore-size distribution were successfully synthesized via facile hydrothermal and post-thermal treatments. The 'soft' cube-like Co_3O_4 granules (Co_3O_4 HMNS) exhibited much higher electrochemical performance than a commercial Co_3O_4 powder with the particle size of ~1-2 μm.

Keywords: A. chemical preparation; D. Spinels; D. Transition metal oxides;
E. Functional applications; Mesoporous material; Micro-octahedra

1. Introduction

Co_3O_4 is a well-known p-type semiconductor [1] and has a normal spinel crystal structure, which contains Co (II) ions in tetrahedral sites and Co (III) ions in octahedral sites [2]. Due to its good electrochemical activity and corrosion resistance in an alkaline condition, Co_3O_4-based materials attract much attention for various applications such as electrocatalysts, environmental purification catalysts, gas sensors, lithium ion batteries and supercapacitors [3-7]. In general,

* Corresponding author: Faculty of Pure and Applied Sciences, University of Tsukuba, Ibaraki 305-8573, Japan.
E-mail address: suzuki@ims.tsukuba.ac.jp (Y. Suzuki).

sufficiently wide active interface area between electrode and electrolyte are required toward these applications, and thus, relatively high specific surface area and accessible pores are necessary for the Co_3O_4-based materials.

To meet above requirements, many kinds of nano- and microscale particle morphologies have been investigated such as various nanostructures and hierarchical micro- and nanostructures (HMNS). As Co_3O_4 nanostructures, for instance, nanorod [8], nanowire [9], nanocube [10,11], nanosheet [12], nanoplate [13] and nanooctahedron [14] have been reported. These well-designed nanostructures are usually synthesized by solution processes followed by post-thermal decomposition; in a typical manner, cobalt-based precursors (cobalt hydroxide or cobalt hydroxide carbonate) are prepared by a sol-gel or hydrothermal treatment, and then they are converted into Co_3O_4 nanostructures. Meanwhile, as Co_3O_4 HMNS, micrometer-sized porous Co_3O_4 have been reported by several groups [15-17]. Li *et al.* [15] reported a star-like structure assembled with Co_3O_4 nanoneedles. Zheng *et al.* [16] reported a flower-like structure assembled with Co_3O_4 nanosheets. Li *et al.* [17] reported a hollow cube-like structure assembled with Co_3O_4 nanosheets. These studies suggest that the Co_3O_4 HMNS are promising for electrochemical applications, *e.g.*, lithium ion batteries and supercapacitors.

Here, we report a unique Co_3O_4 HMNS, *viz.*, micrometer-sized mesoporous granules assembled with Co_3O_4 facetted nanocrystals. This new structure was obtained by a facile hydrothermal synthesis followed by post-thermal decomposition. In order to examine the merits of this unique microstructure, supercapacitor properties were evaluated for Co_3O_4 HMNS and commercial Co_3O_4 powders.

2. Experimental

2.1. Synthesis of a new Co_3O_4 HMNS

Commercially available cobalt chloride hexahydrate ($CoCl_2 \cdot 6H_2O$, Wako, Japan, >99%) and urea (NH_2CONH_2, Wako, Japan, >99%) were weighed to molar ratio of Co : urea = 2:15. These powders were dissolved in 30 mL of a water/ethanol mixed solution (25 mL of distilled water and 5 mL of ethanol) by magnetic stirring for ~10 min. The obtained homogenous pink-colored solution was transferred into a 50 mL Teflon-lined autoclave and hydrothermally heated at 160°C for 0.5 h, 4 h and 6 h. Each precipitate was washed with distilled water and ethanol for several times and dried in an oven at 80°C for ~6 h. The three precursors with different hydrothermal durations were denoted as Co_{pre}-0.5 h, Co_{pre}-4 h and Co_{pre}-6 h, respectively. And then, these three precursors were calcined at 350°C for 3 h in air, resulting three post-thermal decomposition products (i.e., Co_3O_4 HMNS), Co_{post}-0.5 h, Co_{post}-4 h and Co_{post}-6 h.

2.2. Materials characterization

Phase compositions of precursors and calcined powders were characterized by X-ray diffraction (XRD; Multiflex, Cu-Kα, 40 kV and 40 mA, Rigaku). Microstructures of calcined powders were observed by a scanning electron microscope (SEM, JSM-5600U, JEOL) and a field-emission scanning electron microscope (FE-SEM, SU-70, Hitachi High-Technologies). Specific surface areas and pore-size distributions of calcined powders were measured by nitrogen adsorption/desorption (Autosorb-3-AG, Quantachrome) and analyzed by BET and BJH methods. Thermal decomposition behavior of precursor powders was measured by thermogravimetric-differential thermal analysis (TG–DTA, Seiko, TG/DTA7300, 50-550°C, 5°C/min, air atmosphere).

2.3. Electrochemical characterization

As an example of electrochemical properties, supercapacitor properties were evaluated. A three-electrode method was used for the evaluation with an electrochemical analyzer (660A-G, ALS); saturated calomel electrode (SCE) was used as a reference electrode, Pt plate was used as a counter electrode, and a 3 M KOH aqueous solution was used as an electrolyte. As sample powders, synthesized Co_{post}-4 h powder and a commercially available Co_3O_4 powder (specific surface area: ~1 m^2/g, Wako, Japan) were evaluated. The working electrodes were prepared with these sample powders on a Ni foam (2 cm × 1 cm). The Ni foam was immersed in a 3 M HCl solution and cleaned by an ultrasonication for 20 min to remove the oxide layer. It was carefully washed with distilled water, ethanol and acetone. Then, each sample powder was loaded on the cleaned Ni foam with ethanol, and was annealed at 350 ˚C for 3 h. Obtained electrodes were carefully washed with ethanol. The sample mass of the Co_{post}-4 h and the commercial Co_3O_4 powders on the Ni foam was determined to be ~3.2 and ~8.3 mg/cm^2-Ni foam, respectively. These working electrodes were evaluated by cyclic voltammetry (CV) and galvanostatic charge-discharge (GCD) test.

3. Results and Discussion

3.1. Constituent phases of precursors and post-treated products

Figure 1 shows XRD patterns of (a) three precursors with different hydrothermal durations and (b) obtained three Co_3O_4 products after post thermal treatment. As shown in Fig. 1(a), the precursor powder Co_{pre}-0.5 h was identified as $Co(OH)_x(CO_3)_{0.5(2-x)}\cdot nH_2O$ [8]. Note that a representative composition of this hydrous cobalt hydroxide carbonate is reported as $Co(CO_3)_{0.5}(OH)\cdot 0.11H_2O$ (JCPDS No.48-0043). On the other hand, both the precursor powders Co_{pre}-4 h and Co_{pre}-6 h were identified as a single phase $CoCO_3$ (JCPDS No.11-0692). At this stage, the results for Co_{pre}-4 h and Co_{pre}-6 h are similar to a previous work on the solvothermal

synthesis of Co_3O_4 by Jing et al. [18]. As shown in Fig. 1(b), all the post treatment products were identified as a single phase of Co_3O_4 (JCPDS No. 42-1467), which means cobalt precursors were completely converted. To study the thermal decomposition behavior, thermogravimetry-differential thermal analysis (TG-DTA) was conducted (see **Figure S1**).

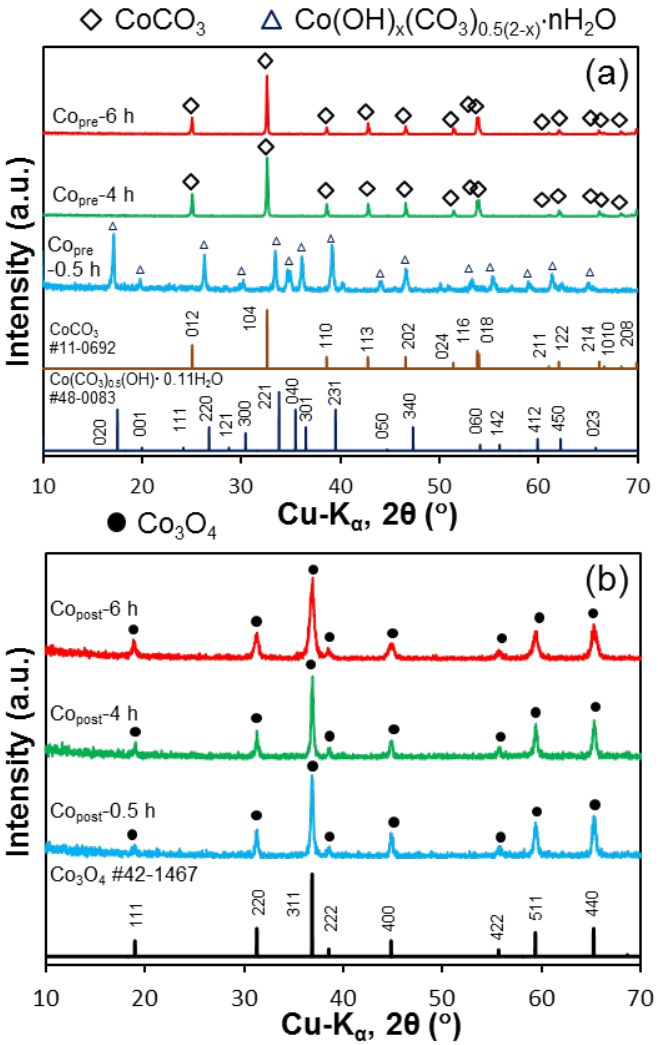

Fig. 1 XRD patterns of (a) three precursors with different hydrothermal durations and (b) obtained three Co_3O_4 products after post thermal treatment.

3.2. Microstructure development of precursors

Figure 2 shows SEM images of the precursors at different hydrothermal durations. Co_{pre}-0.5 h consisted of rod-like $Co(OH)_x(CO_3)_{0.5(2-x)}\cdot nH_2O$ particles. Co_{pre}-2 h consisted of both rod-like $Co(OH)_x(CO_3)_{0.5(2-x)}\cdot nH_2O$ particles and porous 'soft' cube-like $CoCO_3$ particles. Co_{pre}-4

h consisted of porous 'soft' cube-like $CoCO_3$ particles only. And finally, Co_{pre}-6 h consisted of porous 'hard' cube-like $CoCO_3$ particles only. Throughout these SEM observation, initially formed $Co(OH)_x(CO_3)_{0.5(2-x)}\cdot nH_2O$ precursor particles gradually lose the hydroxyl groups and the molecular H_2O, and they rearranged into larger cube-like $CoCO_3$ particles.

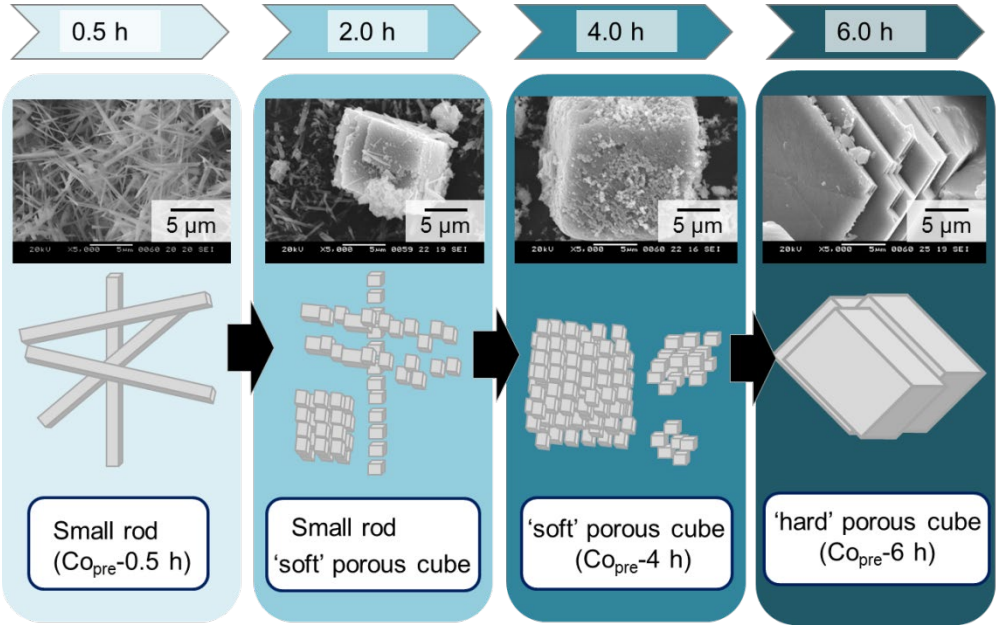

Fig. 2 Microstructure development of precursors at different hydrothermal durations.

3.3. Microstructure of Co_3O_4 HMNS products

Figure 3 shows SEM images of the post thermal treated products. In Figs. 3(a) and (d), Co_{post}-0.5 h, a mixture of micrometer sized rod-like Co_3O_4 particles and nanometer sized equiaxed Co_3O_4 particles were observed. The latter equiaxed particles were probably formed by the thermal decomposition from the former rod-like particles. From the observation of these products, the outer shape of most particles reflected the original shapes of the precursors.

In Figs. 3(b), (e) and (g), Co_{post}-4 h, cube-like granules of ~5-20 μm with rough surface were observed. These 'soft' cube-like granules (keeping the original shape of $CoCO_3$ precursor) were actually the assembly of well-facetted Co_3O_4 microcrystals, as clearly shown in Fig. 3 (g). From this SEM observation, the Co_{post}-4 h sample will be a hierarchical meso-/macroporous material with pore-size of ~10-100 nm.

In Figs. 3(c), (f) and (h), Co_{post}-6 h, cube-like granules of ~20-40 μm with apparently smooth surface were observed. These 'hard' cube-like granules (also keeping the shape of $CoCO_3$ precursor) were composed of fine and equiaxed Co_3O_4 nanocrystals, as clearly shown in Fig. 3 (h). From this SEM observation, the Co_{post}-6 h sample will be a mesoporous material with

uniform pore-size of ~10 nm. Further detail of microstructures of Co_{post}-4 h and Co_{post}-6 h are given in **Fig. S2**.

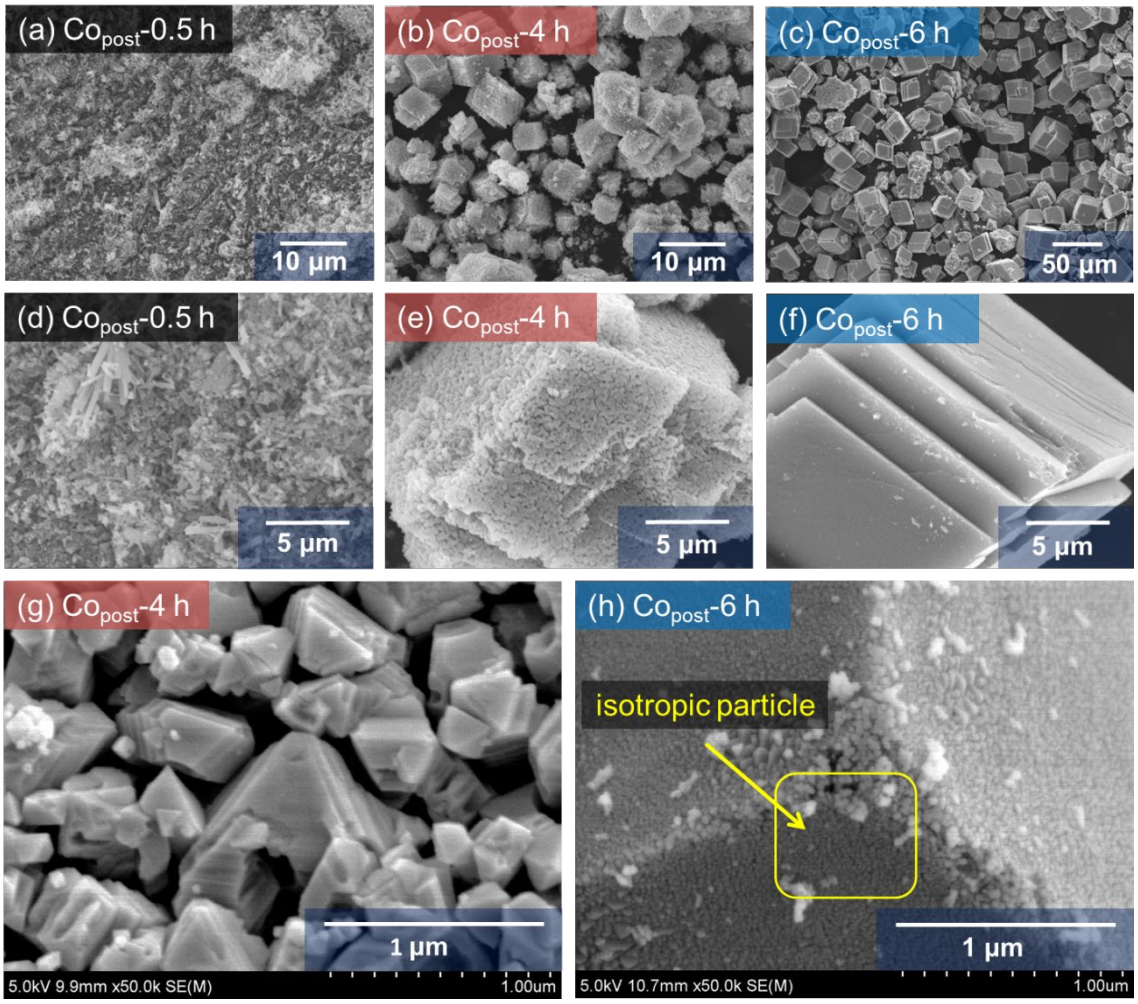

Fig. 3 SEM images of the post thermal treated products (after calcination at 350°C for 3 h): (a), (d) Co_{post}-0.5 h; (b), (e), (g) Co_{post}-4 h; (c), (f), (h) Co_{post}-6 h.

Figure 4 shows N_2 adsorption/desorption isotherms and BJH pore-size-distribution. In Fig. 4(a), all post-treated products had IUPAC type-IV isoterms, which indicates they were mesoporous materials. From Fig. 4 (a) insert, the specific surface areas for Co_{post}-0.5 h, Co_{post}-4 h and Co_{post}-6 h were 23.2, 20.5 and 46.4 m^2/g, respectively. The higher surface area for Co_{post}-6 h is in good agreement with the existence of nanoparticles confirmed by the SEM observation (Fig. 3(h)).

From the desorption isotherms, pore-size-distributions were calculated using BJH analysis as shown in Fig. 4(b). The BJH curves clearly show the existence of mesopores. The typical pore size for Co_{post}-0.5 h, Co_{post}-4 h and Co_{post}-6 h are estimated to be ~20 nm or more,

10-50 nm and ~10 nm, respectively. The pore-size distributions for Co_{post}-4 h and Co_{post}-6 h are in good agreement with the high-resolution SEM observation (Fig. 3 and Fig. S2); the wide pore-size distribution for Co_{post}-4 h corresponds to the interspacing of facetted Co_3O_4 microcrystals (see Fig. 3 (g)) , while the sharp pore-size distribution for Co_{post}-6 h corresponds to the nanoscale voids among Co_3O_4 nanoparticles (see Fig. 3 (h)) . The formation of mesopores in the cubic-like granules can be mainly attributable to the emission of H_2O and CO_2 gases. It is deduced that the crystallinity of the precursor $CoCO_3$ will affect the final pore-size distribution.

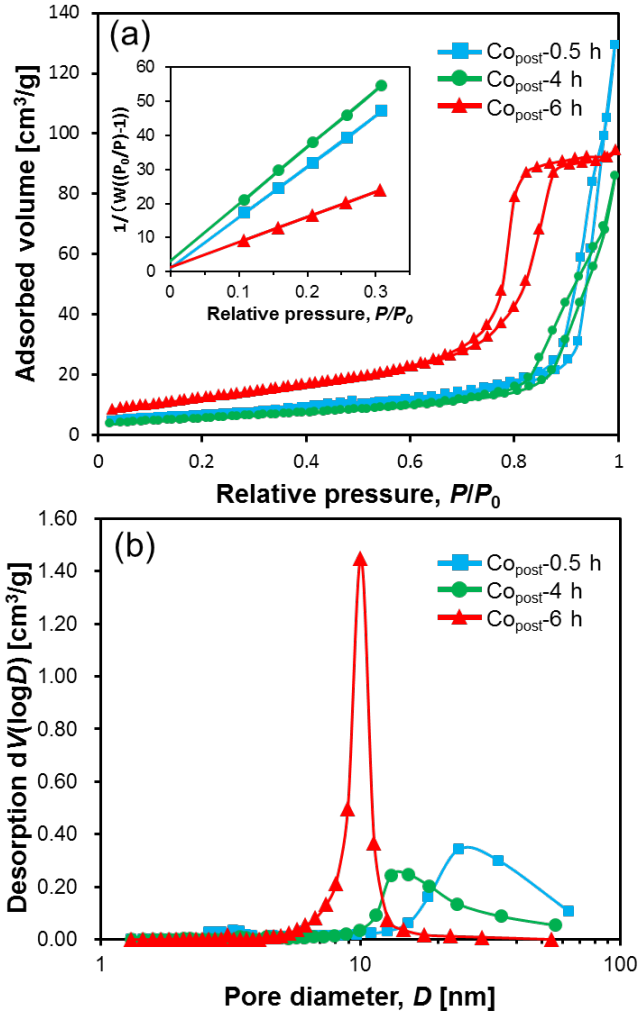

Fig. 4 N_2 adsorption/desorption measurements of the post thermal treated products (after calcination at 350°C for 3 h): (a) isotherms and BET plots, and (b) BJH pore-size-distribution.

3.4. Supercapacitor properties

Figure 5 (a) and (b) show CV curves with different scan rates at 5, 10, 20, 40 and 50 mV s^{-1} in the potential from -0.3 to 0.7 V for commercial Co_3O_4 sample and Co_{post}-4 h HMNS sample. They exhibited pairs of charge-discharge reactions as following equations [19]:

$$Co_3O_4 + OH^- + H_2O \leftrightarrow 3CoOOH + e^- \quad (1)$$

$$CoOOH + OH^- \leftrightarrow CoO_2 + H_2O + e^- \quad (2)$$

Moreover, the anodic and cathodic peaks shifted as the increase of the scan rate in the both samples. This indicates the quasi-reversible redox features.

The Co_3O_4 HMNS powders showed much larger CV curves than the commercial Co_3O_4 powder, which indicates the enhanced electrochemical properties.

Figure 5 (c) and (d) show GCD curves for commercial Co_3O_4 sample and Co_{post}-4 h HMNS sample.The specific capacitance can be calculated by the following formula [20]:

$$C = \frac{I \times \Delta t}{m \times \Delta V} \quad (3)$$

where, C (F g^{-1}) represents the specific capacitance of the working electrode, I (A) refers to the charge/discharge current, Δt (s) is the discharge time, m (g) is the mass of active material and ΔV (V) is potential drop during discharge. By the calculation, the specific capacitance of the commercial Co_3O_4 electrode were quite small, *i.e.*, 2.3, 2.2, 1.9, 1.9, 1.6 and 1.3 F/g at 2, 4, 6, 8, 10 and 15 mA/cm^2, respectively. On the other hand, those of the hierarchical Co_3O_4 electrode were 332.6, 286.3, 266.0, 252.7, 231.1 and 215.2 F/g at 2, 4, 6, 8, 10, and 15 mA/cm^2, respectively, which are ~140 times higher than the commercial powder sample. This is probably because the Co_3O_4 HMNS has a pore structure of ~10-50 nm, so that the electrolyte can be sufficiently immersed in the inside of the macroscopic particles, thereby promoting the electrode reaction activity. Judging from these CV and GCD measurement, the Co_3O_4 HMNS, i,e. 'soft' cube-like Co_3O_4 granules, exhibited much higher electrochemical performance than a commercial Co_3O_4 powder.

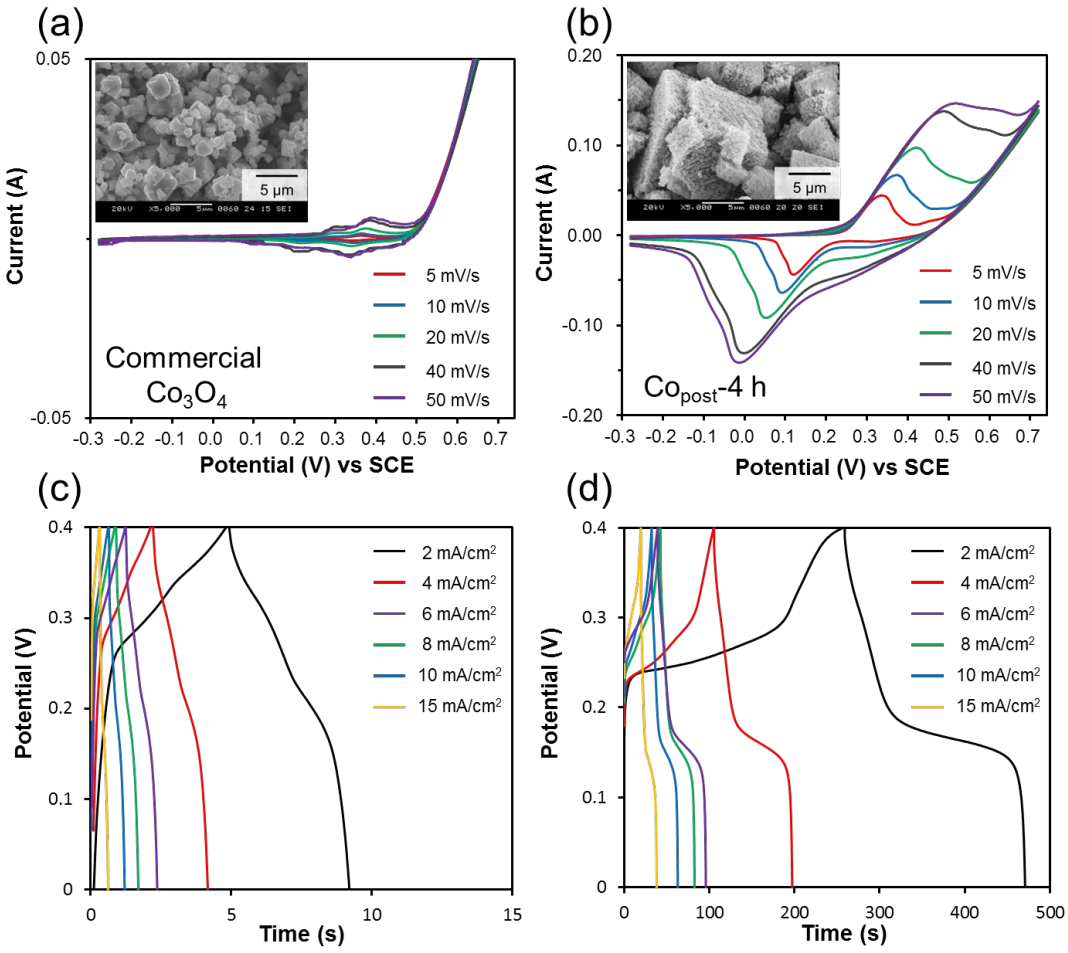

Fig. 5 Cyclic voltammetry (CV) with different scan rates at 5, 10, 20, 40 and 50 mV s^{-1} in the potential from -0.3 to 0.7 V and galvanostatic charge-discharge (GCD) curves of (a, c) commercial Co_3O_4 sample and (b, d) Co_{post}-4 h HMNS sample, respectively.

4. Conclusions

In this study, we reported a unique Co_3O_4 hierarchical micro- and nanostructures, *viz.*, micrometer-sized mesoporous granules assembled with Co_3O_4 facetted nanocrystals via facile hydrothermal treatment and post-thermal decomposition. The product made from $CoCl_2 \cdot 6H_2O$: urea = 2:15 (in mol fraction) by the hydrothermal treatment at 160°C for 4 h followed by the post-thermal treatment at 350°C for 3 h was composed of 'soft' cube-like granules of ~5-20 μm with rough surface, which actually was the assembly of well-facetted Co_3O_4 microcrystals with pore-size distribution of ~10-100 nm. Meanwhile, the other product just by changing the hydrothermal duration for 6 h was composed of 'hard' cube-like granules of ~20-40 μm with apparently smooth surface, which actually was the assembly of fine and equiaxed Co_3O_4

nanocrystals with narrow pore-size of distribution of ~10 nm. Throughout this study, macro and mesoporous Co_3O_4 powders with controlled pore-size distribution were successfully synthesized via facile hydrothermal and post-thermal treatment, and these materials will be applied for the electrochemical energy applications. The Co_3O_4 HMNS exhibited much higher electrochemical performance than a commercial Co_3O_4 powder.

Acknowledgment

This work was supported by JSPS KAKENHI Grant Number JP16H04212 for Basic Research: Category B, and Joint Research Project of JWRI, Osaka University. We thank the Open Facility Network Office, Research Facility Center for Science and Technology, University of Tsukuba, for the SEM observation, TG-DTA and electrochemical measurements.

References

[1] A. Gulino, G. Fiorito, I. Flagala, Deposition of thin films of cobalt oxides by MOCVD , J. Mater. Chem. 13 (2003) 861-865. https://doi.org/10.1039/B211861K

[2] C. Mocuta, A. Barbier, G. Renaud, CoO(111) surface study by surface X-ray diffraction, Appl. Surf. Sci. 162–163 (2002) 56-61. https://doi.org/10.1016/S0169-4332(00)00170-7

[3] H. Osgood, S.V. Devaguptapu, H. Xu, J. Cho, G. Wu, Transition metal (Fe, Co, Ni, and Mn) oxides for oxygen reduction and evolution bifunctional catalysts in alkaline media, Nano Today 11 (2016) 601-625. https://doi.org/10.1016/j.nantod.2016.09.001

[4] Y. Dong, K. He, L. Yin, A. Zhang, A facile route to controlled synthesis of Co_3O_4 nanoparticles and their environmental catalytic properties, Nanotech. 18 (2007) 435602-435607. https://doi.org/10.1088/0957-4484/18/43/435602

[5] Q. Zhou, W. Zeng, Shape control of Co_3O_4 micro-structures for high-performance gas sensor, Physica E 95 (2018) 121-124. https://doi.org/10.1016/j.physe.2017.09.009

[6] B. Li, H. Cao, J. Shao, G. Li, M. Qu, G. Yin, Co_3O_4@graphene Composites as Anode Materials for High-Performance Lithium Ion Batteries, Inorg. Chem. 50 (2011) 1628-1632. https://doi.org/10.1021/ic1023086

[7] C.D. Lokhande, D.P. Dubal, O. Joo, Metal oxide thin film based supercapacitors, Curr. Appl. Phys. 11 (2011) 255-270. https://doi.org/10.1016/j.cap.2010.12.001

[8] R. Xu, H.C. Zeng, Dimensional control of cobalt-hydroxide-carbonate nanorods and their thermal conversion to one-dimensional arrays of Co_3O_4 nanoparticles, J. Phys. Chem. B 107 (2003) 12643-12649. https://doi.org/10.1021/jp035751c

[9] Y. Li, B. Tan, Y. Wu, mesoporous Co_3O_4 nanowire arrays for lithium ion batteries with high capacity and rate capability, Nano Lett. 8 (2008) 265-270. https://doi.org/10.1021/nl0725906

[10] R. Xu, H.C. Zeng, Self-generation of tiered surfactant superstructures for one-pot synthesis of Co_3O_4 nanocubes and their close- and non-close-packed organizations, Langmuir, 20 (2004) 9780-9790. https://doi.org/10.1021/la049164+

[11] L. Hu, K. Sun, Q. Peng, B. Xu, Y. Li, Surface active sites on Co_3O_4 nanobelt and nanocube model catalysts for CO oxidation, Nano Res 3 (2010) 363-368. https://doi.org/10.1007/s12274-010-1040-2

[12] Q. Yang, Z. Lu, X. Sun, J. Liu, Ultrathin Co_3O_4 nanosheet arrays with high supercapacitive performance, Sci. Rep. 3 (2013) 3537-3543. https://doi.org/10.1038/srep03537

[13] L. Li, Y. Chu, J. Song, D. Wang, X. Du, A facile hydrothermal route to synthesize novel Co_3O_4 nanoplates, Mater. Lett. 62 (2008) 1507-1510. https://doi.org/10.1016/j.matlet.2007.09.012

[14] Y. Teng, L.X. Song, L.B. Wang, J. Xia, Face-raised octahedral Co_3O_4 nanocrystals and their catalytic activity in the selective oxidation of alcohols, J. Phys. Chem. C 118 (2014) 4767–4773. https://doi.org/10.1021/jp412175t

[15] L. Li, K.H. Seng, Z. Chen, Z. Guo, H.K. Liu, Self-assembly of hierarchical star-like Co_3O_4 micro/nanostructures and their application in lithium ion batteries, Nanoscale 5 (2013) 1922-1928. https://doi.org/10.1039/C2NR33223J

[16] J. Zheng, J. Liu, L.V. Dongping, Q. Kuang, Z. Jiang, Z. Xie, R. Huang, L. Zheng, A facile synthesis of flower-like Co_3O_4 porous spheres for the lithium-ion battery electrode, J. Solid. State. Chem. 183 (2010) 600–605. https://doi.org/10.1016/j.jssc.2009.12.017

[17] L. Li, Z. Zhang, S. Ren, B. Zhang, S. Yang, B. CaO, Construction of hollow Co_3O_4 cubes as a high-performance anode for lithium ion batteries , New J. Chem. 41 (2017) 7960-7965. https://doi.org/10.1039/c7nj01432e

[18] X. Jimg, S. Song, J. Wang, L. Ge, S. Jamil, Q. Liu, T. Mann, Y. He, M. Zhang, H. Wei, L. Liu, Solvothermal synthesis of morphology controllable $CoCO_3$ and their conversion to Co_3O_4 for catalytic application, Pow. Tech. 217 (2012) 624-628. https://doi.org/10.1016/j.powtec.2011.11.040

[19] I.G. Casella, M. Gatt, Study of the electrochemical deposition and properties of cobalt oxide species in citrate alkaline solutions, J. Electroanal. Chem. 534 (2002) 31−38. https://doi.org/10.1016/S0022-0728(02)01100-2

[20] L. Feng, Y. Zhu, H. Ding, C. Ni, Recent progress in nickel based materials for high performance pseudocapacitor electrodes, J. Power Sources 267 (2014) 430-444. https://doi.org/10.1016/j.jpowsour.2014.05.092